

SAR SHORELINE PROCESSOR: METHODOLOGY AND FIRST RESULTS

*Salvatore Savastano*¹, *Mark E. Pattle*¹, *Albert Garcia-Mondéjar*¹, *Victor Estella-Perez*²,
*Paula Gomes da Silva*³, *Jara Martínez Sánchez*³, *Andres Payo*⁴, *Yeray Castillo*⁵ and *Xavier Monteys*⁵

¹isardSAT Ltd, Guildford, UK ²Lobelia Earth, Barcelona, Spain ³IHCantabria, Santander, Spain
⁴British Geological Survey, Nottingham, UK ⁵Geological Survey Ireland, Ireland

ABSTRACT

Coastlines are continuously transforming, and satellite-based remote sensing represents a cost-effective observation method able to accurately map and monitor these changes. While optical technology is limited by factors like darkness, clouds, and rain, Synthetic Aperture Radar (SAR) remains unaffected, offering the advantage of potentially providing more frequent updates for shoreline mapping. This study presents an innovative automatic processor to extract shorelines (SLs) from SAR data to track coastline variations over time. It is applied across various sites, showing the effects on the SL positions of the incidence angle between the sensor's line of sight and the scene topography. The research findings consistently show that SAR-derived SLs align with positions above the high-water mark across all the studied sites. Depending on the topography, the SLs acquired in ascending (ASC) and descending (DESC) tracks show overlapping or displacement. This paper presents several examples of such occurrences. This offers coastal scientists and stakeholders a unique tool for complementing the analysis conducted by optical sensors, which is especially relevant in regions of the Earth that are constantly affected by cloud cover.

Index Terms— SAR, coastal erosion, Earth Observation, remote sensing, shoreline, incidence angle.

1. INTRODUCTION

Coastal regions experience various transformations caused by both natural forces and human activities. Global concerns are growing regarding the possible risks affecting people, ecosystems, and the environment [1]. Understanding dynamics of these areas and forecasting their future behaviors is essential for making well-informed planning choices. Accurately measuring the alterations in coastal boundaries at different timescales (rapid changes following storms or human interventions, seasonal or interannual erosion or accretion patterns, long term climate change affects) is fundamental in this pursuit. For the last 38 years, remote sensing and satellite technology have shown their potential in monitoring coastal regions, providing a wide

amount of historical shoreline data across different spatial scales. Numerous studies have assessed the effectiveness of satellite-derived shorelines from optical sensors in detecting coastal changes [2, 3]. Conversely, there has been less focus on utilizing SLs derived from SAR, resulting in limited research dedicated to developing and evaluating their accuracy [4, 5]. This paper presents an initial enhancement of a novel processor designed to generate SLs from SAR data [6], aiming to optimize the amount of available data with this technology, which is instrumental for the analysis of short and medium term changes. The algorithm is tailored for publicly available satellite imagery (Sentinel-1 (S1) in C-band) but it can be extended to sensors operating across different frequencies. Given the available polarizations for this sensor and in line with the quantitative analysis proposed in [7], the Vertical-Horizontal (VH) polarization is the preferred choice for use in the processor. Working in all weather conditions and independently from the sunlight, S1 provides very high spatial (10m x 10m) and temporal (6 days revisit time) resolution, allowing to monitor the coastal evolution with hundreds of free available satellite data under the Copernicus program. This aspect represents the main strength of SAR technologies compared to optical images that are unusable for such applications when the Area of Interest (AOI) is even partially covered by clouds. In [6] the potentiality of the novel processor, applied in various sites with different environmental scenarios, has been shown, providing in coastal areas with low elevation, rate of annual change derived from SAR data closely corresponding to established reference values. In this paper a further analysis of the effects of the scene topography on the SLs positions and their relation with the incidence angle and surface elevation are assessed.

2. METHODOLOGY

The SAR SL processor, outlined in Figure 1, has been widely described in [6]. Here a summary of it is reported. The processing is composed by three stages.

Firstly, in the Georeferencing stage, a georeferenced image is generated for each available S1 data, separately for

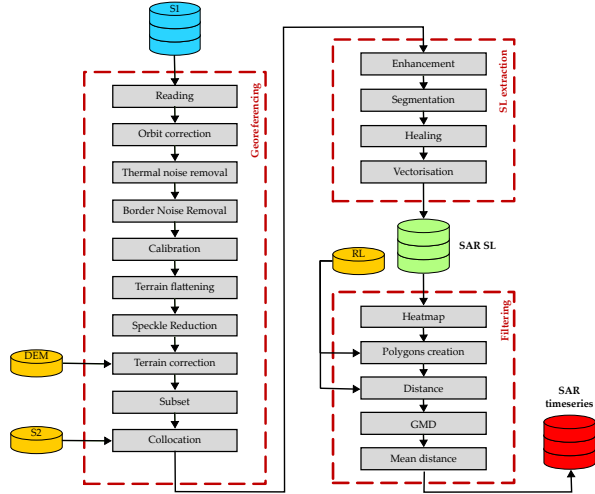


Fig. 1: SAR processing flowchart used in this study showing the three main consecutive steps of Georeferencing, SL extraction and Filtering.

ASC and DESC tracks. This process, accomplished through multiple sub-steps within the SNAP toolbox provided by ESA [8], aims to prepare the data for subsequent analysis. The second stage, known as SL Extraction, consists of four steps: Enhancement, Segmentation, Healing, and Vectorization. The objective here is to improve the quality of the output, reducing as much as possible the erroneous features that may appear in the initial estimation of the SL. The stage generates a vector line, called shoreline from each SAR image, which represents the boundary between land and water. This segmentation is based on the calculation of an appropriate intensity threshold, employing the Kittler method [9]. The resulting SL consists of a sequence of points identified by their geographic coordinates (latitude-longitude) and their respective local incidence angles and elevation. Finally in the third stage of the process (SL filtering), a novel approach has been developed to adequately select points along the previously extracted SAR SLs, creating a refined final product capable of capturing shoreline change patterns over time. The new method is composed of five steps:

1. Heatmapping provides information regarding the dispersion of the SLs and aids in identifying relevant patterns in the scene. For further reduction of speckle, an initial filter based on the heatmap values may be applied removing points located far from the main concentration of SLs.
2. Polygons creation divides the scene into a series of adjacent polygons along a Reference Line (RL), either user-provided or derived from heatmap observations of SL concentration values. The width (w) of polygons can be adjusted on user preferences, while their length (l) is determined by SL distribution or user specifications.
3. Distance (d_i) is attributed for each polygon to all the points along the SL from the RL, within the boundaries of the respective polygon. Moreover, a sign is associated with the distance depending on the location of the point respect to the RL (positive for seaward position, negative for landward position).
4. Gaussian Mixture Distribution (GMD) model is adopted to describe statistically the SL distances. The appropriate number of components for fitting data is determined using the Bayes Information Criterion (BIC) [10]. Once the optimal number of components is determined, the Gaussian distribution with the largest population is considered and its mean (μ_d) and standard deviation (σ_d) are calculated in a way that only distances d_i that satisfy the following expression are considered:
$$\mu_d - 2\sigma_d \leq d_i \leq \mu_d + 2\sigma_d \quad (1)$$
5. Mean distance computation aggregates filtered distance points associated with each SL within individual polygons, providing distinct values representing the SL position. A timeseries of these values is generated from all SLs, enabling detection of shoreline changes over time. Additionally, linear regression is applied to filtered SLs mean values within each polygon, determining the change rate (CR), expressed in m/year. The slope's positive or negative sign signifies accretion or erosion over time, respectively.

3. RESULTS

The results show the high potentiality of using SAR SLs for monitoring coastal evolution, providing more usable SLs compared to the limited data obtained by optical sensors. These SAR SLs are particularly valuable in sites that experience frequent cloud cover and extreme met-ocean conditions throughout most of the year. A full description of the results is presented in [6], and the authors invite the reader to delve into the comprehensive analysis and findings reported therein. In summary the main findings are listed here:

- Thanks to the novel heatmap filtering method, the most of the SLs and points along them are kept and not discarded like some works suggest using met-ocean data to select just images less affected by speckle noise due to the sea conditions [4].
- There is a good coherence between the SAR SLs and the ground truth data available at the study sites, although a full interpretation of SAR's coastal detections remains under development.
- The findings show that SAR SLs used to generate timeseries and change rates are all located above the high-water mark across all the sites, indicating they are not simply detecting the water's edge. The VH configuration

used in the processor leads to believe that SAR SLs are detecting the boundaries between dry and wet sand. However, further analysis is ongoing to confirm this hypothesis.

- The scene geometry (such as flat beach, cliffs, dunes, etc.) is a key element to understand the similarity/discrepancies between the SLs positions from ASC and DESC tracks.

4. INCIDENCE ANGLE ANALYSIS

To investigate and better understand the effects of the topography on SAR SLs positions, an analysis of the local incidence angles associated with each SL point is presented here (Figure 2). The SAR processor has been applied to Pals Beach in Catalonia, Spain, situated along the Costa Brava (Figure 2a). The 3.5 km-long coastline alternates between flat areas and coastal dunes formed by the accumulation of wind-blown sand, and cliffs, providing a valuable site to analyze the correlation between the SAR signal and ground geometry, especially in areas affected by geometric distortions. This analysis includes the processing of all available SAR images from June 2014 to April 2024. The area is illuminated by two ASC tracks (n. 59 and 132) and one DESC (n. 37), producing a total of 926 SLs (596 ASC and 330 DESC). Table 1 shows how the incidence angle (θ_i)

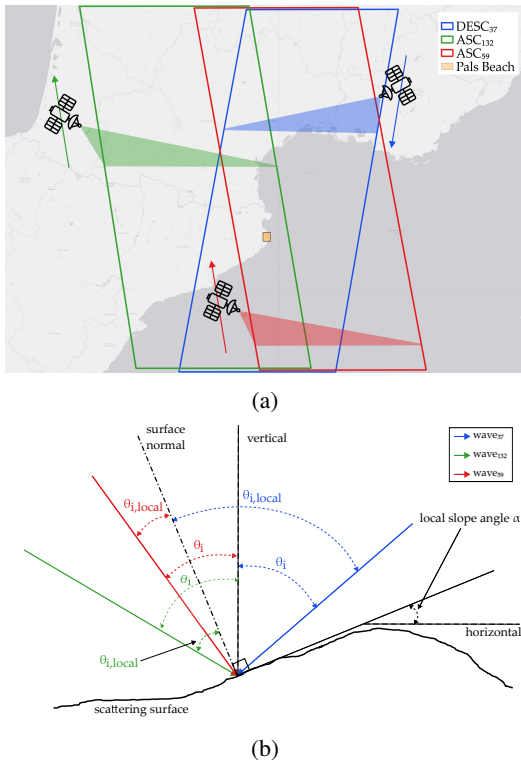


Fig. 2: SAR geometry in Pals Beach: (a) Acquisition geometry from satellite. (b) Local imaging geometry at the scattering surface.

for each track varies across the swath width of the SAR image, from near range (closest to the sensor) to far range (farthest from the sensor), and its value along Pals Beach, which depends on its position relative to the acquisition track. Generally, the interaction of the radar waves from the

Table 1: Summary of the incidence angles for each track covering Pals Beach.

Track	Swath interval	Pals Beach
ASC ₅₉	30.5° – 46.0°	34°
ASC ₁₃₂	30.5° – 46.2°	44°
DESC ₃₇	30.3° – 46.3°	40°

satellite with the scattering surface is illustrated in Figure 2b. For a flat surface, θ_i and local incidence angle ($\theta_{i,local}$) coincide while for a slope θ_i and $\theta_{i,local}$ differ depending on the local slope angle α .

As described in the methodology section, a series of polygons, totaling 142 in number and each with a width of 50 meters and a length of 200 meters, are created along Pals Beach. For this analysis, only two of these polygons (one representing a flat area and the other a non-flat area) are discussed (Figure 3). The heatmap filtering retains only the points crossed by at least three SLs, removing potential noise sources from the main concentration of the SLs. In the polygon 68 (Figure 3a)), all points, independently from track (ASC or DESC), cover the same area, while in the polygon 21 (Figure 3b), there is a clear displacement with DESC points more inland and ASC more towards the sea.

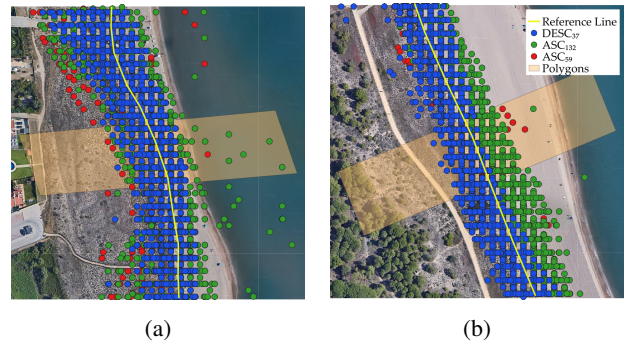


Fig. 3: Points along the SLs in polygons n. 68 (a) and n. 21 (b). Source of aerial imagery: Google, ©2023 Maxar Technologies.

This visual inspection is confirmed by Figure 4, which shows histograms of the elevation associated with each point. Their Overlapping Coefficients (OC) are very high (99%) in the flat area (0m elevation) (Figure 4a), whereas in the second case (Figure 4b), the OC is high only for the two ASC tracks, indicating that the points cover different areas within the same polygon. To illustrate the interaction of the SLs with the elevation profile, the profile tool in QGIS (ver.

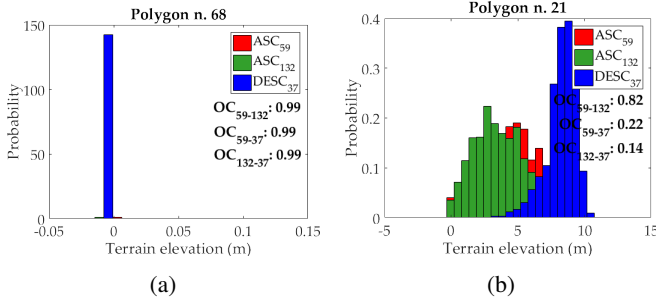


Fig. 4: Histograms and OC for all the tracks in polygon n. 68 (a) and n. 21 (b).

3.28.5-Firenze) [11], considering the same DEM [12] used in SNAP for terrain correction, has been applied to both polygons and the results are shown in Figure 5. Again, in the first case there is a good overlap between ASC and DESC SLs (Figure 5a), covering the same area. However, in the presence of a change in elevation (~ 10 m), the DESC SLs are located more on the top of the hill, while the ASC SLs are more displaced towards the sea (Figure 5b). This mismatch (~ 20 m) may be due to geometric distortion (shadow effect) affecting only the ASC SLs.

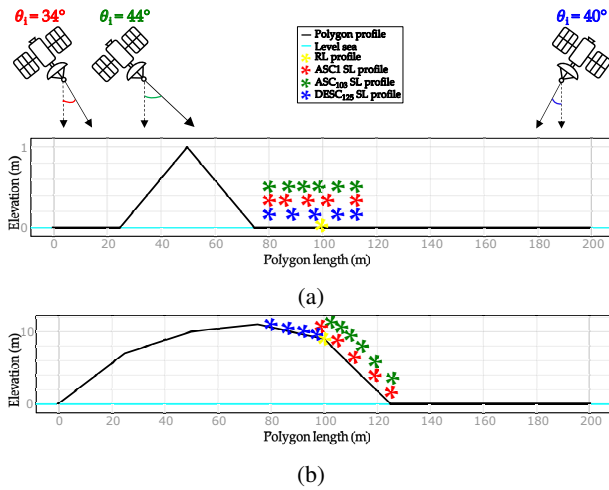


Fig. 5: Polygon profile n. 68 (a) and n. 21 (b).

Finally, Figure 6 illustrates how the incidence angle changes with the topography. In a polygon with a flat beach, θ_i and $\theta_{i, local}$ are identical (Figure 6a), while they differ in a non-flat beach, showing a reduction for DESC and an increase for ASC SLs in accordance with the local slope angle (Figure 6b).

This analysis provides an additional step in understanding what SAR detects along the coast. It represents, a starting point for a new automatic processing approach (currently under development) to combine results from ASC and DESC, aiming to provide end users with a single timeseries and one change rate.

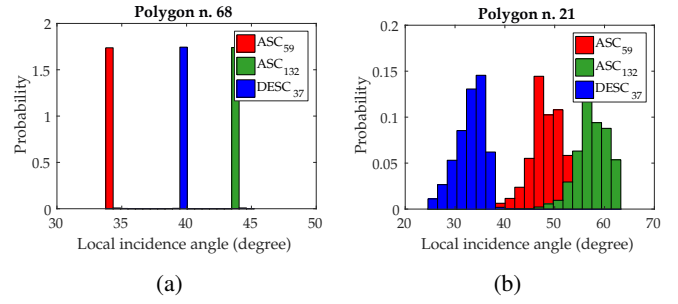


Fig. 6: Local incidence angle distributions in polygon n. 68 (a) and n. 21 (b).

5. CONCLUSIONS

An innovative methodology for monitoring coastal changes using SAR images has been presented. It offers a rich amount of usable data derived by employing a novel approach to filter SAR SLs, independently of the sea conditions.

As reported in a previous publication [6], in specific coastal settings, such as a low-lying beach, SAR-SL proves to be an effective tool for monitoring coastal changes. Furthermore, it has been observed that SAR-SL detection is influenced by various factors, including coastline orientation, coastal topography, radar signal incidence angle, backshore type, and soil moisture.

To better understand one of these factors, in this paper, an analysis of the effects of topography and incidence angle on SAR-based SL detection has been presented. Our research findings consistently show that SAR-derived SLs align with positions above the high-water mark across all the studied sites. Depending on the topography, the SLs acquired in ASC and DESC tracks show overlapping or mismatch. These findings lay the groundwork for a comprehensive approach to utilizing SAR in various coastal types, beyond simply combining results from ASC and DESC tracks, and addressing the challenges posed by geometric distortions. This represents a significant step towards a new method for accurately monitoring coastal changes across different environments.

6. ACKNOWLEDGEMENTS

We would like to acknowledge the funding received by the European Union's Horizon 2020 research and innovation programme under grant agreement No. 101037084 (IMPETUS). AP contribution was supported by the Natural Environment Research Council [grant number NE/Y503265/1]. The contribution by IHCantabria forms part of the ThinkInAzul programme and was supported by Ministerio de Ciencia e Innovación with funding from European Union NextGeneration EU (PRTR-C17.I1) and by Comunidad de Cantabria.

7. REFERENCES

- [1] Jonathan Mingle, *The Ocean and Cryosphere in a Changing Climate: Special Report of the Intergovernmental Panel on Climate Change (IPCC)*, Cambridge University Press, 2022.
- [2] K. Vos, K. D. Splinter, J. Palomar-Vázquez, J. E. Pardo-Pascual, J. Almonacid-Caballer, C. Cabezas-Rabadán, E. C. Kras, A. P. Luijendijk, F. Calkoen, L. P. Almeida, D. Pais, A. H. F. Klein, Y. Mao, D. Harris, B. Castelle, D. Buscombe, and S. Vitousek, “Benchmarking satellite-derived shoreline mapping algorithms,” *Communications Earth & Environment*, vol. 4, no. 1, pp. 345, 2023.
- [3] Paula Gomes da Silva, Martínez Sánchez Jara, Raúl Medina, Anne-Laure Beck, and Mohamed Amine Taji, “On the use of satellite information to detect coastal change: Demonstration case on the coast of Spain,” *Coastal Engineering*, vol. 191, pp. 104517, 2024.
- [4] Yoshimitsu Tajima, Lianhui Wu, Takashi Fuse, Takenori Shimozone, and Shinji Sato, “Study on shoreline monitoring system based on satellite SAR imagery,” *Coastal Engineering Journal*, vol. 61, no. 3, pp. 401–421, 2019.
- [5] Sara Zollini, Donatella Dominici, Maria Alicandro, María Cuevas-González, Eduard Angelats, Francesca Ribas, and Gonzalo Simarro, “New methodology for shoreline extraction using optical and radar (SAR) satellite imagery,” *Journal of Marine Science and Engineering*, vol. 11, no. 3, 2023.
- [6] Salvatore Savastano, Paula Gomes da Silva, Jara Martínez Sánchez, Arnau Garcia Tort, Andres Payo, Mark E. Pattle, Albert Garcia-Mondéjar, Yeray Castillo, and Xavier Monteys, “Assessment of shoreline change from SAR satellite imagery in three tidally controlled coastal environments,” *Journal of Marine Science and Engineering*, vol. 12, no. 1, 2024.
- [7] Sara Zollini, Maria Alicandro, María Cuevas-González, Valerio Baiocchi, Donatella Dominici, and Paolo Massimo Buscema, “Shoreline extraction based on an active connection matrix (ACM) image enhancement strategy,” *Journal of Marine Science and Engineering*, vol. 8, no. 1, 2020.
- [8] Luis Veci, Jun Lu, Michael Fomelis, and Marcus Engdahl, “ESA’s Multi-mission Sentinel-1 Toolbox,” in *EGU General Assembly Conference Abstracts*, Apr. 2017, EGU General Assembly Conference Abstracts, p. 19398.
- [9] J. Kittler and J. Illingworth, “Minimum error thresholding,” *Pattern Recognition*, vol. 19, no. 1, pp. 41–47, 1986.
- [10] Gideon Schwarz, “Estimating the Dimension of a Model,” *The Annals of Statistics*, vol. 6, no. 2, pp. 461–464, 1978.
- [11] QGIS Development Team, *QGIS Geographic Information System*, Open Source Geospatial Foundation, 2024.
- [12] NASA JPL, “Nasa shuttle radar topography mission global 1 arc second, 2013, distributed by NASA EOSDIS Land Processes Distributed Active Archive Center,” <https://doi.org/10.5067/MEASURES/SRTM/SRTMGL1.003> [Accessed: (2024-05-21)].